

Photodecomposition of trimethyltin halides: a theoretical study

N. Ben Amor, C. Daniel *

Laboratoire de Chimie Quantique, UMR 7551 CNRS, Université Louis Pasteur, 4 Rue Blaise Pascal, 67000 Strasbourg, France

Received 26 July 2001; accepted 15 October 2001

Contents

Abstract	11
1. Introduction	11
2. Computational details	12
3. Results and discussion	12
3.1 Excited states	12
3.2 Absorption spectrum	13
3.3 Potential energy curves	13
4. Conclusion	14
Acknowledgements	15
References	15

Abstract

The photodecomposition of $(\text{CH}_3)_3\text{SnI}$, representative of the main group metal complexes $(\text{CH}_3)_3\text{SnX}$ ($\text{X} = \text{Cl}, \text{I}, \text{Br}$) leading to the homolytic cleavage of the $\text{Sn}-\text{X}$ bond in different media (hexane, ethanol, hexanol, porous Vycor glass) under UV irradiation, has been investigated through CASSCF/MS-CASPT2 calculations of the low-lying excited states and associated potential energy curves. The lowest allowed $a^1A' \rightarrow a^1A''$ and $a^1A' \rightarrow b^1A'$ transitions calculated at 42 210 and 42 920 cm^{-1} , respectively correspond to $5p(\text{I}) \rightarrow \sigma_{\text{Sn-I}}^*$ excitations. They contribute to the absorption observed in the experimental spectrum around 235 nm (42 550 cm^{-1}). A strong absorption calculated at 55 610 cm^{-1} ($a^1A' \rightarrow c^1A'$) and corresponding to the $\sigma_{\text{Sn-I}} \rightarrow \sigma_{\text{Sn-I}}^*$ excitation has been assigned to the intense band observed below 200 nm (50 000 cm^{-1}). The potential energy curves associated with the a^1A'' and b^1A' states are dissociative with respect to the $\text{Sn}-\text{I}$ bond elongation leading exclusively to the radicals primary products $[(\text{CH}_3)_3\text{Sn}^\bullet + \bullet\text{I}]$ in an adiabatic scheme. In contrast the upper c^1A' state is quasi-bound with respect to the $\text{Sn}-\text{I}$ bond elongation with a minimum around 4.7 Å generated by a weak avoided crossing between this state and the a^1A' electronic ground state. The upper state correlates to the ionic primary products $[(\text{CH}_3)_3\text{Sn}^+ + \text{I}^-]$. The theoretical spectrum simulated by wavepacket propagations on the low-lying non-adiabatically coupled singlet excited states reflects the main features of the experimental one. © 2002 Elsevier Science B.V. All rights reserved.

Keywords: Photodecomposition; CASSCF/MS-CASPT2; Trimethyltin halides

1. Introduction

In a recent experimental study [1,2] of the photodecomposition of main group metal complexes it was shown that 254 nm excitation of $(\text{CH}_3)_3\text{SnI}$ leads to the

homolytic cleavage of the $\text{Sn}-\text{I}$ bond. This primary process occurs either in non-polar solvents where the system is a four-coordinate tetrahedral complex or in polar media such as ethanol, hexanol or adsorbed onto porous Vycor glass, where the complex exists as a five-coordinate solvent adduct or adsorbate. The absorption spectra show little change as a function of the media and the experimental data point to the ligand-to-metal-charge-transfer (LMCT) character of the pho-

* Corresponding author. Tel.: +33-390241302; fax: +33-390241589.

E-mail address: daniel@quantix.u-strasbg.fr (C. Daniel).

toactive state. This electronic excited state is less polarized than the electronic ground state and is thought to lead to the radicals formation because of this more uniform charge distribution. The quantum yield Φ of the homolytic splitting of the Sn–I bond is wavelength dependent with values varying between 0.32 ($\lambda_{\text{exc}} = 254$ nm) and less than 10^{-3} with $\lambda_{\text{exc}} = 350$ nm.

In order to establish the correlation between the photoactive state and the nature of the primary products, a theoretical study has been undertaken on the basis of highly correlated quantum chemical calculations. The aim of the present contribution is to determine the low-lying transitions to the singlet states and the corresponding oscillator strengths as well as the one-dimensional associated potential energy curves (PEC) calculated as a function of the [$q_a = \text{Sn-I}$] coordinate. The complete-active-space SCF (CASSCF) [3] wavefunctions are used as zero-order references in a subsequent 2nd order perturbative treatment of the dynamical correlation effects through the multi-state complete-active-space PT2 (MS-CASPT2) method [4]. The calculations have been performed with the MOLCAS 5.0 Quantum Chemistry software [5].

2. Computational details

Ab initio calculations have been performed for a nearly T_d structure (Fig. 1) under the C_s symmetry constraint with the following bond lengths and angles optimized at the DFT level of theory using the B3LYP functional with GAUSSIAN 98 [6] for the a^1A' electronic ground state:

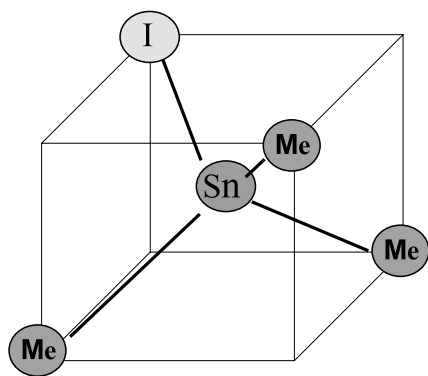
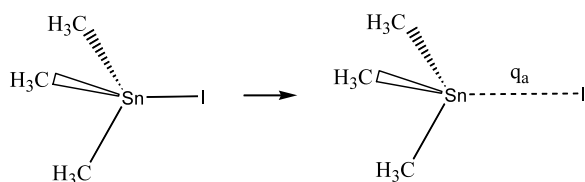


Fig. 1. T_d structure of $(\text{CH}_3)_3\text{SnI}$.



Scheme 1.

$\text{Sn-I} = 2.824 \text{ \AA}$ (2.729 \AA at the MS-CASPT2 level)

$\text{Sn-C} = 2.161 \text{ \AA}$

$\text{C-H} = 1.096 \text{ \AA}$

$\theta_{\text{C-Sn-I}} = 105^\circ$

$\theta_{\text{C-Sn-C}} = 113^\circ$

The photodissociation of the Sn–I bond has been followed under the C_s symmetry constraint without any relaxation of the other degrees of freedom (Scheme 1).

The Sn and I atoms have been described using the relativistic ab initio potential model (CG-AIMP) [7] with the following associated valence basis sets: for the Sn atom ($Z = 14.0$) a (11s, 10p, 7d) set contracted to [3s, 3p, 3d], for the I atom ($Z = 17.0$) a (11s, 10p, 7d) set contracted to [3s, 4p, 3d]. The following atomic natural orbitals ANO [8] basis sets have been used for the C and H atoms in the all-electron scheme: for the C atoms a (10s, 6p, 3d) set contracted to [3s, 2p, 1d] and for the H atoms a (7s, 3p) set contracted to [2s, 1p].

Ten electrons have been correlated in 10 active orbitals in the CASSCF calculations, including mainly the $\sigma_{\text{Sn-C}}$ and $\sigma_{\text{Sn-I}}$ bonding orbitals and their antibonding counterparts $\sigma_{\text{Sn-C}}^*$ and $\sigma_{\text{Sn-I}}^*$ with respect to the Sn–C and Sn–I bonds, respectively together with the $5p_y(\text{I})$ and $5p_x(\text{I})$ of the halide. Other virtual orbitals of mixed character between the methyl groups and the Sn atom are included in the CASSCF active space. The electronic ground state is described by the following electronic configuration $(\sigma_{\text{Sn-C}})^2 (\sigma_{\text{Sn-I}})^2 (5p_y(\text{I}))^2 (\sigma_{\text{Sn-C}}^*)^2 (5p_x(\text{I}))^2$, the first three orbitals belong to the A' symmetry, whereas the last two orbitals have the A'' symmetry. The $^1A'$ and $^1A''$ CASSCF wavefunctions averaged over 10 roots are used as references of the subsequent CASPT2 perturbational treatment of the electronic dynamical correlation effects in the multi-states approach using the level shift corrected perturbation method [9] with a value of 0.2. This method, which has been used in a number of applications [10], allows the determination of the transition energies with accuracy of around 1000 cm^{-1} taking into account the mixing between the different excited states of the same symmetry.

3. Results and discussion

3.1. Excited states

The transition energies to the low-lying singlet excited states of $(\text{CH}_3)_3\text{SnI}$ calculated at the CASSCF/MS-CASPT2 level at the equilibrium distance $\text{Sn-I} = 2.729 \text{ \AA}$ (Franck-Condon) are reported in Table 1 together with the corresponding oscillator strengths.

Table 1
Calculated MS-CASPT2 transition energies (cm^{-1}) to the lowest excited states of $(\text{CH}_3)_3\text{SnI}$ and associated oscillator strengths

Transition	One-electron excitation in the principal configurations	Energy	Oscillator strength
$a^1A' \rightarrow a^1A''$	$5p_x(\text{I}) \rightarrow \sigma_{\text{Sn-I}}^*$	42 210	0.005
$a^1A' \rightarrow b^1A'$	$5p_y(\text{I}) \rightarrow \sigma_{\text{Sn-I}}^*$	42 920	0.012
$a^1A' \rightarrow b^1A''$	$5p_x(\text{Sn}) \rightarrow \sigma_{\text{Sn-I}}^*$	53 220	0.039
$a^1A' \rightarrow c^1A'$	$\sigma_{\text{Sn-I}} \rightarrow \sigma_{\text{Sn-I}}^*$	55 610	0.812

Two sets of excited states characterize the absorption spectrum of this molecule, the first one around $42\,000\text{ cm}^{-1}$ associated with the $a^1A' \rightarrow a^1A''$ and $a^1A' \rightarrow b^1A'$ transitions corresponding mainly to $5p(\text{I}) \rightarrow \sigma_{\text{Sn-I}}^*$ excitations and the second one in the far-UV energy domain (around $55\,000\text{ cm}^{-1}$ or 180 nm) associated with the $a^1A' \rightarrow c^1A'$ and $a^1A' \rightarrow b^1A''$ transitions corresponding to $\sigma_{\text{Sn-I}} \rightarrow \sigma_{\text{Sn-I}}^*$ and $5p(\text{Sn}) \rightarrow \sigma_{\text{Sn-I}}^*$ excitations, respectively. The first two transitions with modest oscillator strengths ($f < 0.015$) should contribute to the first band observed in the experimental absorption spectrum (Fig. 2) around 235 nm , whereas the intense absorption below 200 nm results from the $a^1A' \rightarrow c^1A'$ transition calculated at $55\,610\text{ cm}^{-1}$ with an oscillator strength of 0.812 .

3.2. Absorption spectrum

The theoretical spectrum obtained by Fourier transform of the autocorrelation function deduced from wavepacket propagations on the singlet potential energy curves is represented in Fig. 3 and compares rather well with the experimental spectrum recorded in hexane (Fig. 2).

Obviously, taking into account the solvent effects in the simulation would probably modify the shape of the theoretical spectrum but the environment effects are beyond the scope of the present study.

3.3. Potential energy curves

The CASSCF/MS-CASPT2 potential energy curves calculated for the a^1A' electronic ground state and the low-lying singlet excited states of $(\text{CH}_3)_3\text{SnI}$ as a function of the Sn–I bond elongation, freezing the rest of the molecule are depicted in Fig. 4.

The b^1A' and a^1A'' excited states corresponding to the $5p(\text{I}) \rightarrow \sigma_{\text{Sn-I}}^*$ excitations are dissociative with respect to this coordinate leading directly to the radical primary products $[(\text{CH}_3)_3\text{Sn}^\bullet + \bullet\text{I}]$ without any energy barrier following an adiabatic process. The shape of the potential energy curves associated with the lowest absorbing states around 235 nm explains the efficiency ($\Phi = 0.32$) of the Sn–I bond homolysis upon irradiation at 254 nm . According to preliminary femtosecond dynamics simulations based on wavepackets propagations [11], this process should be completed within 100 fs .

In contrast the upper singlet states c^1A' and b^1A'' are quasi-bound with respect to the Sn–I bond elongation. In particular, the c^1A' state corresponding to the $\sigma_{\text{Sn-I}} \rightarrow \sigma_{\text{Sn-I}}^*$ excitation absorbing strongly around $55\,000\text{ cm}^{-1}$ (180 nm) leads to the ionic primary products $[(\text{CH}_3)_3\text{Sn}^+ + \text{I}^-]$. Moreover, the a^1A' electronic ground state and c^1A' excited state potential energy curves avoid a weak crossing around 4.7 \AA , the ionic primary products correlating with the electronic ground state a^1A' of the reactant $(\text{CH}_3)_3\text{SnI}$ which has a highly polarized character.

On the basis of the shape of the potential energy curves depicted in Fig. 4, one may easily understand why the ionic species cannot be formed upon irradiation into the low energy domain (below $50\,000\text{ cm}^{-1}$). Despite the ionic character of the reactant, one has to populate the c^1A' excited state to induce the Sn–I bond breaking towards the ionic primary products following a non-adiabatic process with a dramatic change of electronic configuration around the avoided crossing at 4.7 \AA . Preliminary wavepacket simulations on the a^1A' and c^1A' coupled potentials in the diabatic scheme [11] predict a dissociation probability of nearly 1.0 towards the ionic species $\text{I}^- + (\text{CH}_3)_3\text{Sn}^+$ in 200 fs .

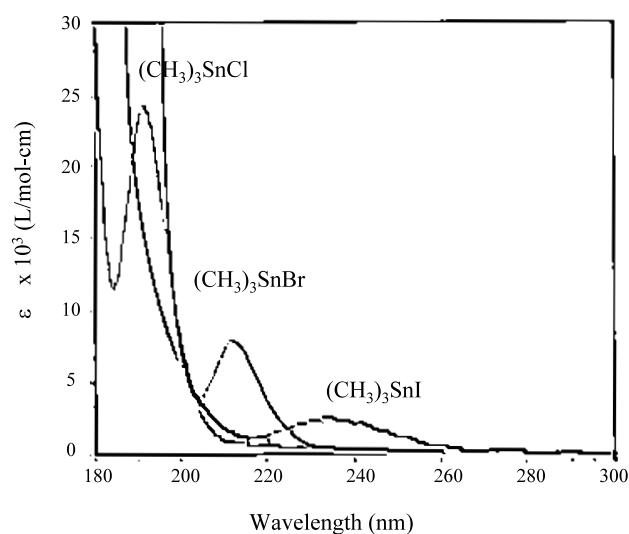


Fig. 2. Experimental absorption spectrum of $(\text{CH}_3)_3\text{SnX}$ ($X = \text{Cl}, \text{I}, \text{Br}$) recorded in hexane [1].

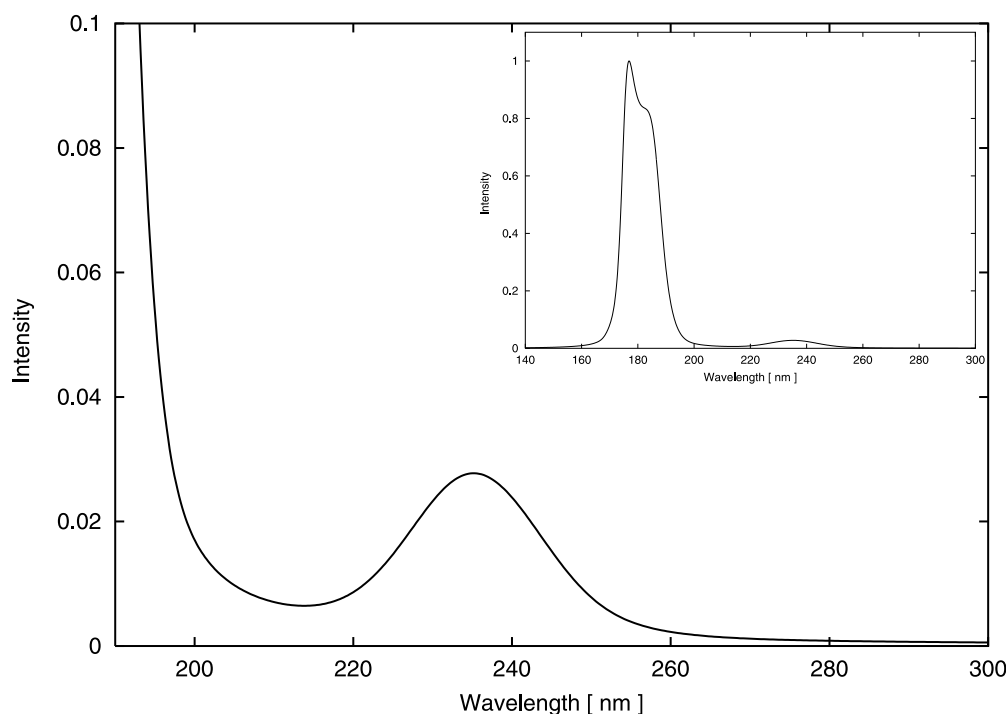


Fig. 3. Theoretical absorption spectrum of $(\text{CH}_3)_3\text{SnI}$ in the UV–far-UV region.

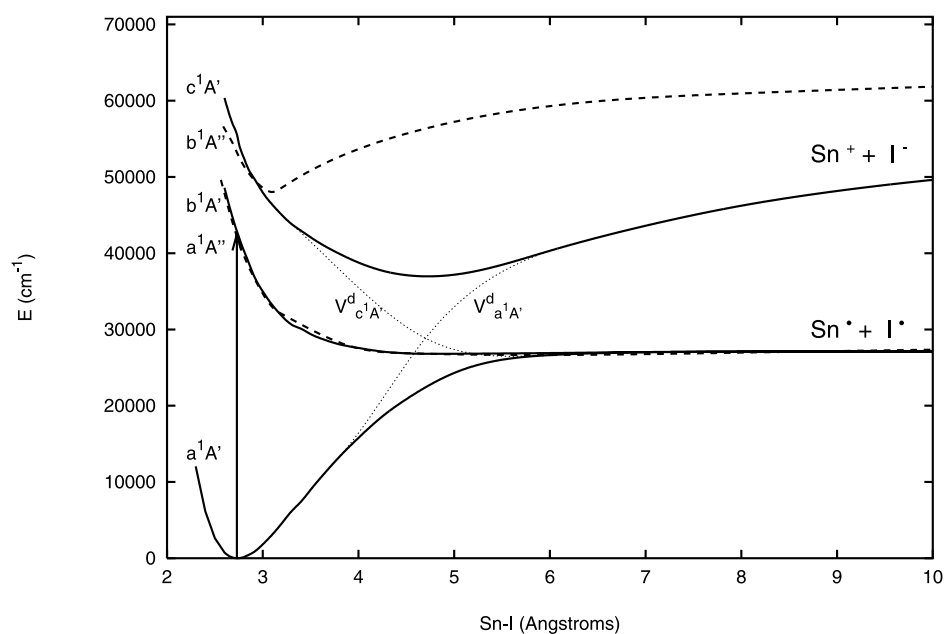


Fig. 4. MS-CASPT2 potential energy curves of $(\text{CH}_3)_3\text{SnI}$ as a function of the Sn–I bond elongation. A' symmetry curves in solid line, A'' symmetry curves in dashed line.

4. Conclusion

On the basis of accurate *ab initio* calculations the lowest part of the absorption spectrum of the trimethyltin iodide has been assigned. The theoretical spectrum which compares rather well with the experimental one exhibits two bands, a shoulder of weak absorption around $42\,000\text{ cm}^{-1}$ (238 nm) corre-

sponding mainly to $5p(\text{I}) \rightarrow \sigma_{\text{Sn-I}}^*$ excitations and an intense band around $55\,000\text{ cm}^{-1}$ (180 nm) corresponding to the $\sigma_{\text{Sn-I}} \rightarrow \sigma_{\text{Sn-I}}^*$ excitation. A qualitative mechanism of photodecomposition of the title metal main group complex is proposed on the basis of the shape of the potential energy curves associated with the electronic ground state and low-lying singlet excited states:

1. vertical absorption into the lowest band of the absorption spectrum (around $40\,000\text{ cm}^{-1}$) will lead exclusively to the formation of the radicals primary products $[(\text{CH}_3)_3\text{Sn}^\bullet + \text{I}^\bullet]$ along a direct fast dissociative adiabatic process;
2. the formation of the ionic primary products $[(\text{CH}_3)_3\text{Sn}^+ + \text{I}^-]$ will result from excitation into the upper part of the absorption spectrum (around $55\,000\text{ cm}^{-1}$) according to a non-adiabatic mechanism, where the electronic ground state is coupled to the photoactive c^1A' state.

Preliminary calculations [11] indicate that the triplet states play a minor role in this mechanism characterized by fast processes (a few hundreds of fs). This mechanism explains the low efficiency of the Sn–I bond homolysis with low wavelengths of irradiation (310 and 350 nm). In contrast to the hypothesis based on the experimental data [1], a qualitative correlation between the orbital nature of the photoactive state and the character (ionic or radicals) of the primary products are difficult to establish. The selective formation of the primary products is entirely controlled by the shape of the potential energy curves and not by the more or less polarized character of the active state. The coupling between the electronic ground state (highly polarized) and the c^1A' ($\sigma_{\text{Sn}-\text{I}} \rightarrow \sigma_{\text{Sn}-\text{I}}^*$) state (less polarized) will be the driving force of the formation of the ionic species. The branching ratio and the efficiency of the primary reactions may probably vary as a function of the experimental conditions (irradiation wavelength, environment effects). Study of the $(\text{CH}_3)_3\text{SnX}$ ($\text{X} = \text{Cl}$ or Br) is in progress. Future theoretical work will take into account the solvent effects and some control of the primary products distribution will be proposed on the basis of laser pulse simulations.

Acknowledgements

The authors are grateful to Professor H.D. Gafney for helpful discussions. The quantum chemical calculations have been carried out at the IDRIS Computer

Centre (Orsay, France) through a grant of computer time from the Conseil Scientifique.

References

- [1] J. Dong, P.S. Devi, D. Sunil, E. Mendoza, H.D. Gafney, *Inorg. Chem.* submitted.
- [2] J. Dong, P.S. Devi, D. Sunil, E. Mendoza, H.D. Gafney, 14th ISPPCC, Veszprém, July 2001.
- [3] B.O. Roos, P.R. Taylor, P.E.M. Siegbahn, *Chem. Phys.* 48 (1980) 157.
- [4] J. Finley, P.-Å. Malmqvist, B.O. Roos, L. Serrano-Andrés, *Chem. Phys. Lett.* 288 (1998) 299.
- [5] K. Andersson, M. Barysz, A. Bernhardsson, M.R.A. Blomberg, D.L. Cooper, T. Fleig, M.P. Fülscher, C. de Graaf, B.A. Hess, G. Karlström, R. Lindh, P.-Å. Malmqvist, P. Neogrady, J. Olsen, B.O. Roos, A.J. Sadlej, M. Schütz, B. Schimmelpfennig, L. Seijo, L. Serrano-Andrés, P.E.M. Siegbahn, J. Ståhring, T. Thorsteinsson, V. Veryazov, P.-O. Widmark, *MOLCAS 5.0*, Lund University, Sweden.
- [6] M.J. Frisch, G.W. Trucks, H.B. Schlegel, G.E. Scuseria, M.A. Robb, J.R. Cheeseman, V.G. Zakrzewski, J.A. Montgomery, Jr., R.E. Stratmann, J.C. Burant, S. Dapprich, J.M. Millam, A.D. Daniels, K.N. Kudin, M.C. Strain, O. Farkas, J. Tomasi, V. Barone, M. Cossi, R. Cammi, B. Mennucci, C. Pomelli, C. Adamo, S. Clifford, J. Ochterski, G.A. Petersson, P.Y. Ayala, Q. Cui, K. Morokuma, D.K. Malick, A.D. Rabuck, K. Raghavachari, J.B. Foresman, J. Cioslowski, J.V. Ortiz, A.G. Baboul, B.B. Stefanov, G. Liu, A. Liashenko, P. Piskorz, I. Komaromi, R. Gomperts, R.L. Martin, D.J. Fox, T. Keith, M.A. Al-Laham, C.Y. Peng, A. Nanayakkara, C. Gonzalez, M. Challacombe, P.M.W. Gill, B. Johnson, W. Chen, M.W. Wong, J.L. Andres, C. González, M. Head-Gordon, E.S. Replogle, *GAUSSIAN 98*, Revision A.7.
- [7] (a) S. Huzinaga, L. Seijo, Z. Barandiarán, M. Klobukowski, *J. Chem. Phys.* 86 (1987) 2132;
(b) L. Seijo, Z. Barandiarán, *J. Chem. Phys.* 101 (1994) 4049.
- [8] K. Pierloot, B. Dumez, P.-O. Widmark, B.O. Roos, *Thror. Chem. Acta* 90 (1995) 87.
- [9] B.O. Roos, K. Andersson, M.P. Fülscher, L. Serrano-Andrés, K. Pierloot, M. Merchán, V. Molina, *J. Mol. Struct. Theochem.* 388 (1996) 257.
- [10] B.O. Roos, K. Andersson, M.P. Fülscher, P.-Å. Malmqvist, L. Serrano-Andrés, K. Pierloot, M. Merchán, in: Ilya Prigogine, S.A. Rice (Eds.), *Advances in Chemical Physics: New Methods in Computational Quantum Mechanics*, vol. XCIII:219, John Wiley & Sons, New York, 1996.
- [11] N. Ben Amor, C. Daniel, in preparation.